The Astrophysical Journal Letters, 884:L38 (7pp), 2019 October 20 https://doi.org/10.3847/2041-8213/ab4799

A New Type of Jet in a Polar Limb of the Solar Coronal Hole

Il-Hyun Cho[1], Yong-Jae Moon[1,2], Kyung-Suk Cho[3,4], Valery M. Nakariakov[2,5,6], Jin-Yi Lee[1], and Yeon-Han Kim[3]
[1] Department of Astronomy and Space Science, Kyung Hee University, Yongin 446-701, Republic of Korea; moonyj@khu.ac.kr
[2] School of Space Research, Kyung Hee University, Yongin 446-701, Republic of Korea
[3] Space Science Division, Korea Astronomy and Space Science Institute, Daejeon 305-348, Republic of Korea
[4] Department of Astronomy and Space Science, University of Science and Technology, Daejeon 305-348, Republic of Korea
[5] Centre for Fusion, Space and Astrophysics, Department of Physics, University of Warwick, CV4 7AL, UK
[6] Special Astrophysical Observatory, Russian Academy of Sciences, St. Petersburg, 196140, Russia
Received 2019 September 9; revised 2019 September 19; accepted 2019 September 20; published 2019 October 15

Abstract

A new type of chromospheric jet in a polar limb of a coronal hole is discovered in the Ca II filtergram of the Solar Optical Telescope on board the *Hinode*. We identify 30 jets in a filtered Ca II movie with a duration of 53 minutes. The average speed at their maximum heights is found to be 132 ± 44 km s^{-1} ranging from 57 to 264 km s^{-1} along the propagation direction. The average lifetime is 20 ± 6 ranging from 11 to 36 s. The speed and lifetime of the jets are located at end-tails of those parameters determined for type II spicules, hence implying a new type of jets. To confirm whether these jets are different from conventional spicules, we construct a time–height image averaged over a horizontal region of 1″, and calculate lagged cross-correlations of intensity profiles at each height with the intensity at 2 Mm. From this, we obtain a cross-correlation map as a function of lag and height. We find that the correlation curve as a function of lag time is well fitted into three different Gaussian functions whose standard deviations of the lag time are 193, 42, and 17 s. The corresponding propagation speeds are calculated to be 9 km s^{-1}, 67 km s^{-1}, and 121 km s^{-1}, respectively. The kinematic properties of the former two components seem to correspond to the 3-minute oscillations and type II spicules, while the latter component to the jets is addressed in this study.

Unified Astronomy Thesaurus concepts: Solar chromosphere (1479); Astronomy data analysis (1858); Solar optical telescopes (1514)

Supporting material: extended figure

1. Introduction

The solar chromosphere is morphologically dominated by spicular jets. It is suggested that there are at least two types of spicules when observed in the Ca II filtergram (de Pontieu et al. 2007b). One is the so-called type I spicules typically observed in active regions. These spicules show a rise and fall, and they have lifetimes of 150–400 s and maximum ascending velocities of 15–40 km s^{-1} (Pereira et al. 2012). Their motion is characterized by a nonballistic and parabolic-like path (de Pontieu et al. 2007b), suggesting that they are driven by shocks (de Pontieu et al. 2007a), which could be observed in fibrils and mottles (Suematsu et al. 1995; Hansteen et al. 2006; Rouppe van der Voort et al. 2007).

The other is type II spicules, which are fast and short-lived compared to type I spicules (de Pontieu et al. 2007b). It was shown that type II spicules, common in the quiet Sun and coronal holes, have lifetimes of 50–150 s, velocities of 30–110 km s^{-1}, and are not seen to fall down, but fade at around their maximum length (Pereira et al. 2012). On the other hand, Zhang et al. (2012) reported that there seems to be no convincing evidence of type-II spicules, and the majority of spicules are type-I spicules. Hence, there is still an ongoing debate about the existence of type-II spicules.

Tian et al. (2014) discovered intermittent small-scale jets in narrow network lanes in the transition region lines with the *Interface Region Imaging Spectrograph* (*IRIS*, De Pontieu et al. 2014). The average speed, lifetime, and recurring period of the network jets were found to be 80–250 km s^{-1}, 20–80 s, and 8.3 minutes, respectively, suggesting they could be a counterpart of Type II spicules. It has been proposed that some of the network jets are propagating heating fronts caused by dissipation of a current-sheet that could be formed during formation of the spicule (De Pontieu et al. 2017). From multiwavelength observations in Ca II H with the Solar Optical Telescope (Tsuneta et al. 2008) on board the *Hinode* (Kosugi et al. 2007), *IRIS* ultraviolet (UV), and extreme ultraviolet filtergrams taken by the Atmospheric Imaging Assembly (AIA; Lemen et al. 2012) on board the *Solar Dynamics Observatory* (*SDO*; Pesnell et al. 2012), it was shown that Ca II spicules often follow only the early, more linear, phase of the parabola and mostly continue their evolution in hotter pass bands after they fade from the Ca II H line (Skogsrud et al. 2015). Loboda & Bogachev (2019) analyzed 330 macrospicules with a lifetime of ∼10 minutes observed in the 304 Å of the *SDO*/AIA. In their study, a part of the macrospicules was found to be inconsistent with a purely ballistic motion as in the type I spicules. But the rise velocity is 70–140 km s^{-1}, which is similar to the speed of type II spicules. One the other hand, Pereira et al. (2012) discovered faint and transient spicules in active regions, whose speed and lifetime are 160 ± 36 km s^{-1} and 37 ± 16 s, respectively. These were interpreted as type II spicules in active regions based on their high velocities and short lifetimes.

In this Letter, we report on a new type of highly transient and recurring jet in a polar coronal hole observed in the Ca II H filtergram. In Section 2, we present data processing. In Section 3, kinematic properties of jets are presented by two different methods. Finally, we summarize and discuss our results in Section 4.

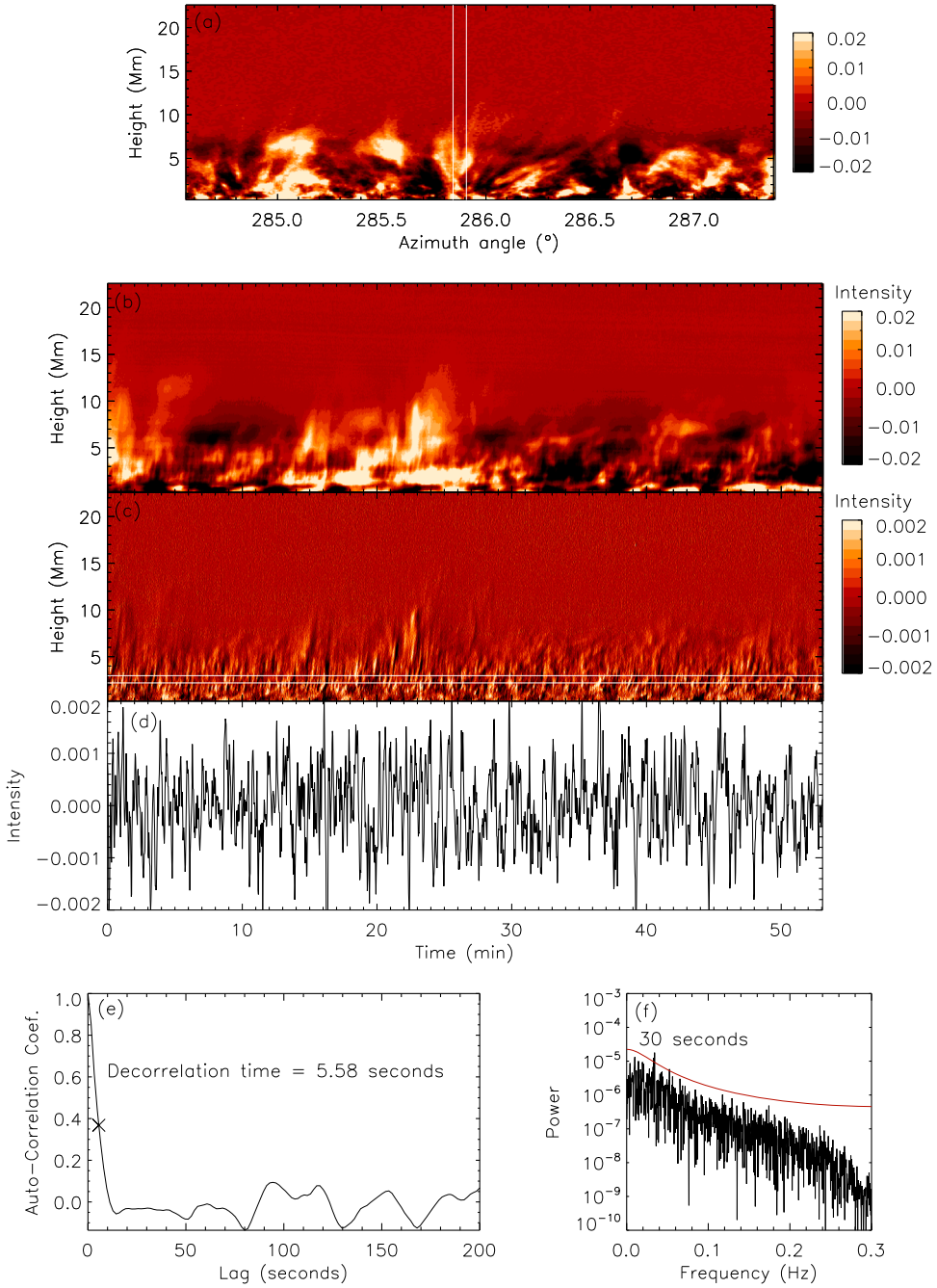

Figure 1. Snapshot of the Ca II filtergram image normalized by the average intensity of the disk region (a), time–height image for the slice defined by two vertical white lines (b), first-order time-difference of the time–height image (c), average intensity time series of the region between two horizontal white lines, which is subtracted by its linear least-square fitting line (d), autocorrelation function of the detrended intensity time series with its decorrelation time (×) (e), and corresponding Fourier power (f). In panel (a), the radial gradient is subtracted from the original image. The red curve in panel (f) is the noise power of 99.9% significance level of the red noise defined by the autoregressive noise model of the order 1.

2. Data

We use the Ca II H filtergrams taken by the *Hinode*/SOT on 2011 January 29 11:06–11:59 UT.[7] The time cadence, pixel resolution, and exposure time are 1.6 s, 0.″109, and ∼0.6144 s, respectively. The wavelength passband of the filtergram is 3968.5 ± 3 Å. The field of view is 56″ × 56″ which is located at the south polar coronal hole. This data has been analyzed by Okamoto & De Pontieu (2011) to explore propagating kink waves along type II spicules lasting longer than 40 s.

We align the image cube by using the disk region, and rotate it to locate limbs approximately parallel to the horizontal line. Then, each image is transformed to the polar coordinate by using bilinear interpolation. In this step, the horizontal and vertical axes of the polar coordinate are defined by sampling positions evenly along a straight line which is normal to the limb for a given position along the limb. There is a very tiny offset in the cadence of 1.6 s. We use a 1.6 s evenly sampled image cube by using the linear interpolation. The intensity is normalized by the mean intensity of the solar disk for a given frame. For a given height, the radial gradient determined from

[7] https://sot.lmsal.com/data/sot/level0/2011/01/29/FG/H1100/

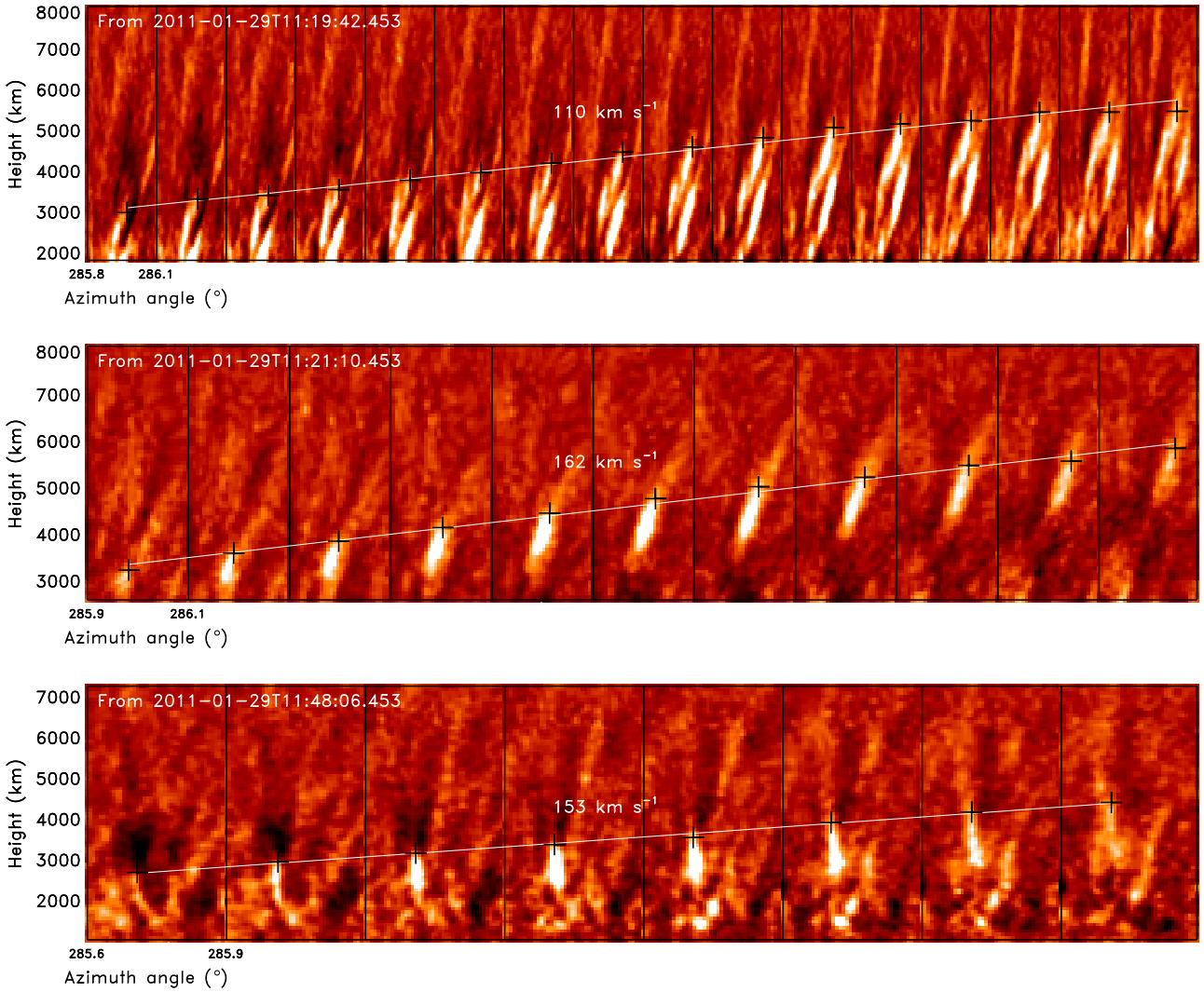

Figure 2. Thirty examples of the evolution of jets at every 1.6 s. The cross symbol represents the maximum height of a jet at each frame. The straight white line is the linear fitting curve of maximum heights, which indicates the speed of jets in the vertical direction. (An extended version of this figure is available.)

the average intensity in the horizontal direction is subtracted (Figure 1(a)).

3. Methods and Results

From the background subtracted (radial gradient) Ca II movie, we recognized that there are very transient, repeated, and fast jet-like flows or eruptions. To identify what they are, we draw the time–height image over a 1″ horizontal region indicated by two vertical white lines in Figure 1(a). As shown in Figure 1(b), many repeated, thin, faint, and inclined straws seem to exist in the time–height image. To quantitatively verify if the straw structures are real, we estimate the Fourier power for the time series of detrended intensity (Figure 1(d)). The detrended intensity is defined as the average of the first-order time differences over the height range of 2–3 Mm indicated by two horizontal white lines in Figure 1(c), and then subtracted by the linear least-square fitting line. The Fourier power seems to be inversely proportional to frequency, and hence we interpret that the time series includes a red noise. The noise power is explicitly given by the autoregressive model of the order 1 (Schulz & Mudelsee 2002) as $P = \sigma^2/(1–2\rho\cos(\pi f/f_N) + \rho^2)$, which follows a chi-square distribution with two degrees of freedom, where σ and ρ are the standard deviation of the time series and the autoregressive parameter, respectively. The autoregressive parameter is determined from the decorrelation time (τ) of the autocorrelation function of the time series, $\rho = e^{-1.6/\tau}$, where 1.6 (s) indicates the sampling interval of the data. The decorrelation time is defined as the time when the autocorrelation is equal to e^{-1} ($\times$ in Figure 1(e)). This approach provides noise powers resembling the power law (e.g., Pugh et al. 2017), where the period is close to the decorrelation time, but provides uniform-like powers as the period locates further away from the decorrelation time. It is found that the powers at frequency equal to $1/(30\,\mathrm{s})$ are apparently higher than the noise level of 99.9% (red curve). The periodicity of 30 s could indicate that the straws appear at every 30 s in the time–height image.

In the following subsections, we identify 30 sets of jet evolutions in the Ca II movie, which were expected from the inclined straws. Independently, we identify three upwardly propagating components in the Ca II movie by a cross-correlation analysis. As the next step, we demonstrate that the kinematics of our jets are different from conventional spicules.

3.1. Kinematics of Faint Jets

Based on the estimated period of the occurrence, the Ca II intensity is subtracted by backgrounds given by a smoothing

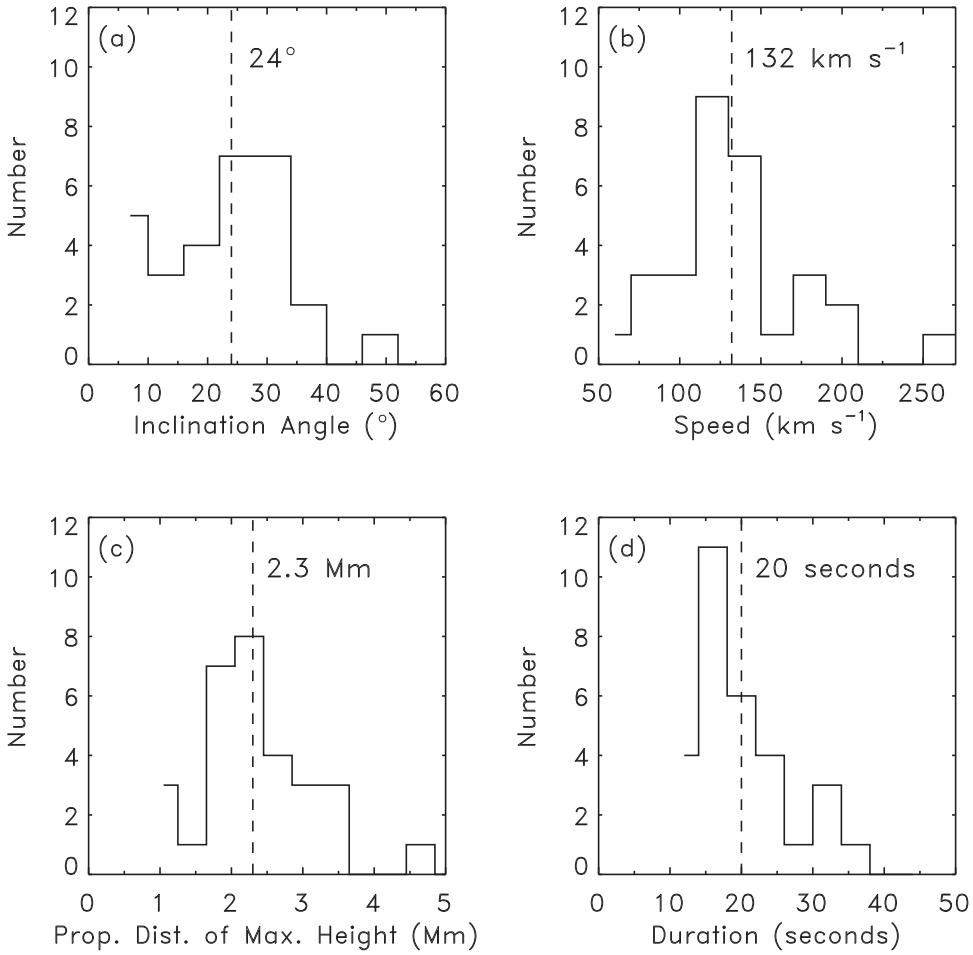

Figure 3. Histograms of (a) inclination angle, (b) speed, (c) propagation distance, and (d) duration of 30 jets. The vertical dashed line in each panel indicates the mean value of the parameter.

window of 30 s at each pixel position. By this process, the temporal variation of type II spicules would be minimized, enhancing a jet-like feature on the plane of the sky, which was expected from the inclined straws in the time–height image. From the background subtracted movie, we identify 30 sets of jet-like evolutions. We determine the maximum heights as a function of time for each jet, and calculate the lifetime as well as the vertical propagation speed of maximum height using a linear least-square fitting. We also determine the inclination angle and propagation distance of maximum height of each jet. Thirty examples are shown in Figure 2.

The histograms of the jet parameters are presented in Figure 3. The inclination angle of the jets is 24° ± 12° and ranges from 4° to 53°. It is found that the propagation distance of maximum heights of the jets is 2.3 ± 0.8 Mm ranging from 0.8–4.6 Mm. The lifetime is 20 ± 6 s ranging from 11–36 s. The speed along the inclined path is calculated to be 132 ± 44 km s^{-1} and ranges from 57 to 264 km s^{-1}. The mean speed is located outside 2σ from the average speed of type II spicules, and the lifetime around 2σ, indicating that the jets are more transient and faster compared to those of type II spicules in the Ca II band (see Pereira et al. 2012). A comparison of the kinematics of the jets discussed here and conventional spicules is presented in Table 1.

Table 1
Comparison of Kinematic Parameters of the Jets

	Type I Spicules[a]	Type II Spicules[b]	New Jets
Inclination Angle (°)	12.7 ± 9.8	15.3 ± 11.1	24 ± 12
Speed (km s^{-1})	30 ± 9	71 ± 29	132 ± 44
Lifetime (s)	262 ± 80	83 ± 35	20 ± 6
Propagation Distance (Mm)	···	···	2.3 ± 0.8
Recurring Period (s)	···	···	30

Notes.
[a] In active regions given by Pereira et al. (2012).
[b] In coronal holes given by Pereira et al. (2012).

3.2. Cross-correlation Analysis of Time–height Images

As mentioned above, the kinematic properties of our jets seem to be located at the high-end tail of the distribution of the II spicules. To examine whether these jets are different from type II spicules, we perform a lagged cross-correlation analysis to identify propagating components of intensity disturbances independently. From the original time–height image shown in Figure 1(b), we calculate the lagged cross-correlation coefficient (CCC) between two intensity profiles across heights

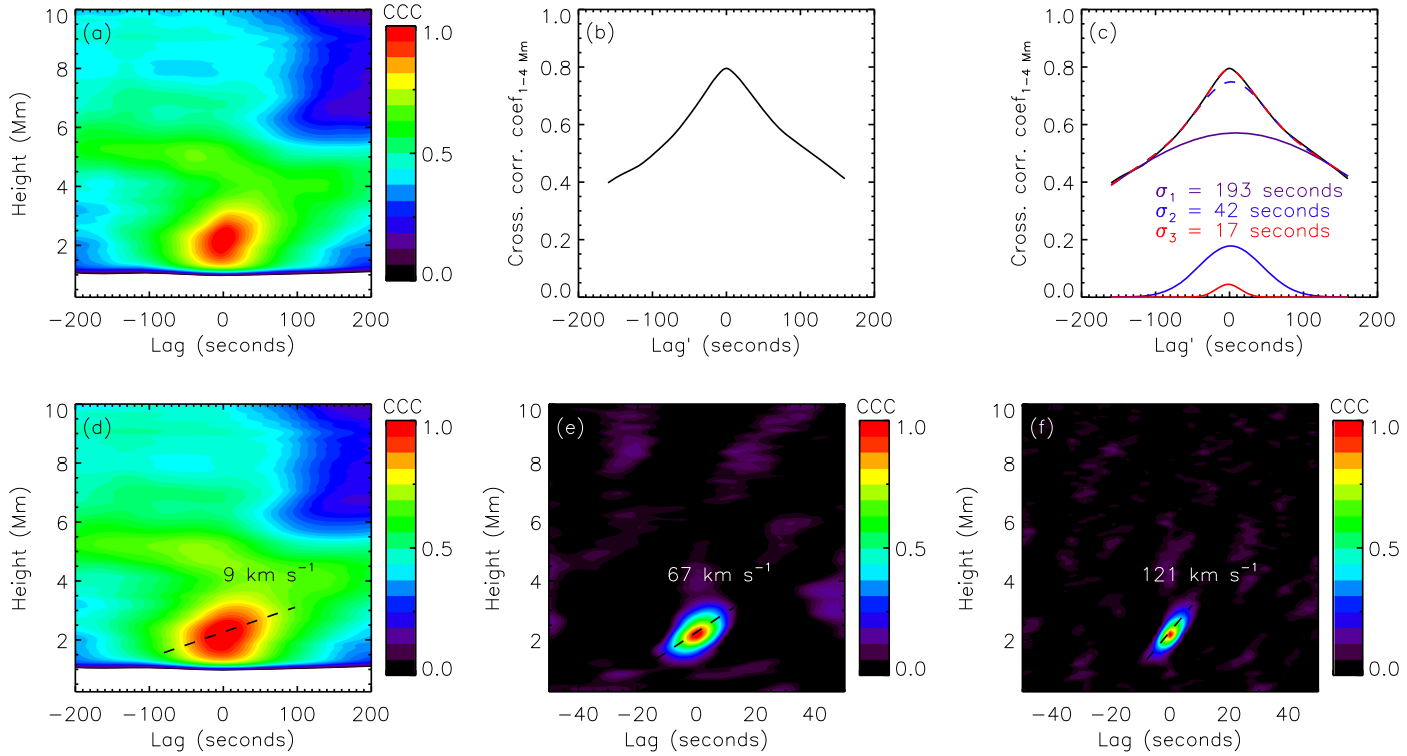

Figure 4. (a) Map of the cross-correlation coefficient (CCC) obtained from the time–height image of Figure 1(b), and (b) the average of CCC in the height range from 1 to 4 Mm. The lagged correlation at each height is calculated from two intensity profiles at the given height and 2 Mm. In panel (c), the purple, blue, and red curves are three Gaussian functions with the standard deviations of 193, 42, and 17 s, respectively. The blue dashed curve is the sum of the former two Gaussian functions. The red dashed curve is the sum of all three functions. The cross-correlation map in panel (d) is obtained from the time–height images of smoothed backgrounds whose width of averaging windows is 193 s. The cross-correlation maps in panels (e) and (f) are obtained from the time–height images subtracted by smoothed backgrounds whose widths of averaging windows are 42 and 17 s. The straight dashed line in panels (d)–(f) indicate the propagation speed of intensity variations in the time–height images.

(Figure 4(a)). One is the intensity profile for a given height, and the other is at a fixed height of 2 Mm. The lag is set from +320 s to −320 s with a 1.6 s interval. We average the correlation coefficients from 1 to 4 Mm as shown in Figure 4(b), with respect to the zero lag for a given height. With this analysis, we expect that at least two propagating components of intensity disturbances would be captured in the correlation map, including type II spicules and our jets.

It is found that the curve is well fitted with a sum of three Gaussian functions (rather than two components) with standard deviations of 193, 42, and 17 s, which are indicated by solid purple, solid blue, and solid red curves, respectively (Figure 4(c)). In Figure 4(c), the dashed blue and dashed red curves represent the sum of the former two Gaussian functions and the sum of all three Gaussian functions, respectively. Note that the solid black line in Figure 4(c) is the same as that in Figure 4(b).

The above analysis may imply that the original time–height image includes three characteristic timescales of different dynamical components. To identify each component in a cross-correlation map, we construct three different time–height images based on the three timescales. One image is obtained from the background of the original time–height image, whose timescale is longer than 193 s. The other two images are background subtracted ones, whose timescales are shorter than 42 s and 17 s, respectively. From these three filtered time–height images, we calculate again the cross-correlations as a function of lag and height referenced by the intensity profile at the fixed height of 2 Mm (Figures 4(d)–(f)). The positive lag for a given height indicates that the intensity profile is lagged to the intensity profile at 2 Mm. The negitive lag indicates that the intensity profile leads to the profile at 2 Mm. Hence, the inclined elliptic contours shown in the correlation maps in Figures 4(d)–(f) represent upward propagations.

The propagation speeds are various in three components. In Figure 4(d), the speed is calculated as 9 km s^{-1}. Interestingly, this speed corresponds to the sound speed of ∼7635 K plasma, that approximates the propagation speed of slow magnetoacoustic waves under a low-β condition (Roberts 2006). This implies that the speed reflects cool chromospheric conditions. In addition, the timescale of 193 s corresponds to the period of chromospheric oscillations. In Figure 4(e), the speed is estimated to be 67 km s^{-1}. Considering the average inclination angle of 24°, the deprojected speed is 73 km s^{-1} which is consistent with the typical speed of type II spicules in coronal holes (72 km s^{-1}) (Pereira et al. 2012). The timescale of 42 s corresponds to the half of the lifetime (83 ± 35 s) of type II spicules in coronal holes (Pereira et al. 2012), we interpret that the second component may reflect the kinematic properties of type II spicules too.

However, the third component gives the speed of 121 km s^{-1} (Figure 4(f)). Considering the inclination angle, the deprojected speed becomes 132.5 km s^{-1}. Interestingly, this value is the same with the speed of jets in our study. In addition, the timescale of 17 s is also consistent with the lifetime of the jets (20 s). Hence, the jets presented in our study likely belong to the third population, which is independent of type II spicules.

4. Summary and Discussion

We provide 30 sets of jet evolutions in the Ca II filtergram taken by *Hinode*/SOT observed from 2011 January 29 11:06–11:59 UT. The occurrence period, propagation speed, and lifetime are 30 s, 132 ± 44 km s^{-1} (57–264 km s^{-1}), and 20 ± 6 s (11–36 s), respectively. The intensity perturbation having similar kinematic properties is detected from the cross-correlation analysis, which is significantly different from the chromospheric oscillations and type II spicules. Hence, we conclude that a new type of jet-like propagating structure exists in the chromosphere that is more transient and faster than typical type II spicules. The intensity is at least 10 times fainter than the typical intensity of the chromospheric structure in the limb as shown in Figures 1(b)–(c), but it seems to occur very frequently (30 s), suggesting that these jets may play a role in the mass supply to the solar wind. On the other hand, the high speeds of these jets are likely not completely caused by mass flows. A significant fraction could be caused by propagating heating fronts (e.g., De Pontieu et al. 2017) or a fast-mode wave (e.g., Kubo et al. 2016). The propagation distance of maximum height of the jets is found to be 2.3 ± 0.8 Mm, suggesting that these jet might not directly contribute to the coronal heating.

Recently, rapid and transient phenomena were reported in the transition region (e.g., Tian et al. 2014; Vissers et al. 2015; Kubo et al. 2016) as well as in the corona (e.g., Testa et al. 2013; Raouafi & Stenborg 2014; Gupta & Tripathi 2015; Samanta et al. 2016; Joshi et al. 2017; DeForest et al. 2018; Panesar et al. 2018). Particularly, Tian et al. (2014) discovered intermittent small-scale jets in narrow network lanes in the *IRIS* transition region lines. The speed, lifetime, and recurring period of the network jets were found to be 80–250 km s^{-1}, 20–80 s, and 8.3 minutes, respectively. The speed and lifetime of the jets in our study are overlapped with those of the network jets. Kubo et al. (2016) discovered ubiquitous fast-propagating intensity disturbances (PIDs) on the Sun by the Lyα transition region line taken by the Chromospheric Lyα SpectroPolarimeter (Kano et al. 2012; Kobayashi et al. 2012). The speed and timescale of the PIDs were found to be 150–350 km s^{-1} and 30 s, respectively, which are overlapped with the jet parameters in this study. Hence, kinematic properties of the Ca II jets in our study may partly be related to the previous observations in the UV bands. On the other hand, the jets in this study are obviously faster than the chromospheric jets (e.g., Shibata et al. 2007; Yang et al. 2013; Cho et al. 2019), which are apparently associated with magnetic reconnections (e.g., Kim et al. 2015; Tian et al. 2016; Seo et al. 2019).

A mechanism responsible for the observed jet evolutions could be a super-Alfvénic flow. A ponderomotive force in a nonlinear torsional Alfvén wave (Vasheghani Farahani et al. 2011; Mozafari Ghoraba & Vasheghani Farahani 2018), which could be generated by magnetic tornadoes observed from the photosphere to the corona (Wedemeyer-Böhm et al. 2012), can produce a longitudinal (directed upwards) perturbation at a super-Alfvénic speed. On the other hand, high-frequency oscillations (e.g., Jess et al. 2007; Zaqarashvili et al. 2007; Morton et al. 2012; Jafarzadeh et al. 2017; Narang et al. 2019) and/or periodic reconnection induced by magnetohydrodynamic waves (e.g., McLaughlin et al. 2012, 2018; Nakariakov et al. 2016; Thurgood et al. 2017; Xue et al. 2019) could be considered responsible for the observed jet occurrence too.

This work is supported by the Korea Astronomy and Space Science Institute under the R&D program "Study on the Determination of Coronal Physical Quantities using Solar Multi-wavelength Images (project No. 2019-1-850-02)" supervised by the Ministry of Science and ICT and the National Research Foundation of Korea (NRF; grant Nos. 2019R1C1C1006033, NRF-2019R1A2C1002634, NRF-2016R1A2B4013131, NRF-2016R1A6A3A11932534), and the BK 21 plus program funded by the Korean Government. This work is also supported by the Institute for Information & Communications Technology Promotion (grant No. 2018-0-01422). V.M.N. acknowledges support from the STFC consolidated grant ST/P000320/1, the Russian Foundation for Basic Research (grant No. 18-29-21016), and the BK 21 plus program.

ORCID iDs

Il-Hyun Cho https://orcid.org/0000-0001-7514-8171
Yong-Jae Moon https://orcid.org/0000-0001-6216-6944
Kyung-Suk Cho https://orcid.org/0000-0003-2161-9606
Valery M. Nakariakov https://orcid.org/0000-0001-6423-8286
Jin-Yi Lee https://orcid.org/0000-0001-6412-5556
Yeon-Han Kim https://orcid.org/0000-0001-5900-6237

References

Cho, K.-S., Cho, I.-H., Nakariakov, V. M., et al. 2019, ApJL, 877, L1
DeForest, C. E., Howard, R. A., Velli, M., Viall, N., & Vourlidas, A. 2018, ApJ, 862, 18
de Pontieu, B., Hansteen, V. H., Rouppe van der Voort, L., van Noort, M., & Carlsson, M. 2007a, in ASP Conf. Ser. 368, Coimbra SolarPhysics Meeting on the Physics of Chromospheric Plasmas, ed. P. Heinzel, I. Dorotovic, & R. J. Rutten (San Francisco: ASP), 65
De Pontieu, B., Martínez-Sykora, J., & Chintzoglou, G. 2017, ApJL, 849, L7
de Pontieu, B., McIntosh, S., Hansteen, V. H., et al. 2007b, PASJ, 59, S655
De Pontieu, B., Title, A. M., Lemen, J. R., et al. 2014, SoPh, 289, 2733
Gupta, G. R., & Tripathi, D. 2015, ApJ, 809, 82
Hansteen, V. H., De Pontieu, B., Rouppe van der Voort, L., van Noort, M., & Carlsson, M. 2006, ApJL, 647, L73
Jafarzadeh, S., Solanki, S. K., Gafeira, R., et al. 2017, ApJS, 229, 9
Jess, D. B., Andić, A., Mathioudakis, M., Bloomfield, D. S., & Keenan, F. P. 2007, A&A, 473, 943
Joshi, N. C., Chandra, R., Guo, Y., et al. 2017, Ap&SS, 362, 10
Kano, R., Bando, T., Narukage, N., et al. 2012, Proc. SPIE, 8443, 84434F
Kim, Y.-H., Yurchyshyn, V., Bong, S.-C., et al. 2015, ApJ, 810, 38
Kobayashi, K., Kano, R., Trujillo-Bueno, J., et al. 2012, in ASP Conf. Ser. 456, Fifth Hinode Science Meeting, 456, ed. L. Golub, I. De Moortel, & T. Shimizu (San Francisco, CA: ASP), 233
Kosugi, T., Matsuzaki, K., Sakao, T., et al. 2007, SoPh, 243, 3
Kubo, M., Katsukawa, Y., Suematsu, Y., et al. 2016, ApJ, 832, 141
Lemen, J. R., Title, A. M., Akin, D. J., et al. 2012, SoPh, 275, 17
Loboda, I. P., & Bogachev, S. A. 2019, ApJ, 871, 230
McLaughlin, J. A., Nakariakov, V. M., Dominique, M., Jelínek, P., & Takasao, S. 2018, SSRv, 214, 45
McLaughlin, J. A., Thurgood, J. O., & MacTaggart, D. 2012, A&A, 548, A98
Morton, R. J., Verth, G., Jess, D. B., et al. 2012, NatCo, 3, 1315
Mozafari Ghoraba, A., & Vasheghani Farahani, S. 2018, ApJ, 869, 93
Nakariakov, V. M., Pilipenko, V., Heilig, B., et al. 2016, SSRv, 200, 75
Narang, N., Pant, V., Banerjee, D., & Van Doorsselaere, T. 2019, FrASS, 6, 36
Okamoto, T. J., & De Pontieu, B. 2011, ApJL, 736, L24
Panesar, N. K., Sterling, A. C., Moore, R. L., et al. 2018, ApJL, 868, L27
Pereira, T. M. D., De Pontieu, B., & Carlsson, M. 2012, ApJ, 759, 18
Pesnell, W. D., Thompson, B. J., & Chamberlin, P. C. 2012, SoPh, 275, 3
Pugh, C. E., Broomhall, A.-M., & Nakariakov, V. M. 2017, A&A, 602, A47
Raouafi, N.-E., & Stenborg, G. 2014, ApJ, 787, 118
Roberts, B. 2006, RSPTA, 364, 447
Rouppe van der Voort, L. H. M., De Pontieu, B., Hansteen, V. H., Carlsson, M., & van Noort, M. 2007, ApJL, 660, L169
Samanta, T., Singh, J., Sindhuja, G., & Banerjee, D. 2016, SoPh, 291, 155
Schulz, M., & Mudelsee, M. 2002, CG, 28, 421

Seo, M., Quintero Noda, C., Lee, J., & Chae, J. 2019, ApJ, 871, 125
Shibata, K., Nakamura, T., Matsumoto, T., et al. 2007, Sci, 318, 1591
Skogsrud, H., Rouppe van der Voort, L., De Pontieu, B., & Pereira, T. M. D. 2015, ApJ, 806, 170
Suematsu, Y., Wang, H., & Zirin, H. 1995, ApJ, 450, 411
Testa, P., De Pontieu, B., Martínez-Sykora, J., et al. 2013, ApJL, 770, L1
Thurgood, J. O., Pontin, D. I., & McLaughlin, J. A. 2017, ApJ, 844, 2
Tian, H., DeLuca, E. E., Cranmer, S. R., et al. 2014, Sci, 346, 1255711
Tian, H., Xu, Z., He, J., & Madsen, C. 2016, ApJ, 824, 96
Tsuneta, S., Ichimoto, K., Katsukawa, Y., et al. 2008, SoPh, 249, 167
Vasheghani Farahani, S., Nakariakov, V. M., van Doorsselaere, T., & Verwichte, E. 2011, A&A, 526, A80
Vissers, G. J. M., Rouppe van der Voort, L. H. M., & Carlsson, M. 2015, ApJL, 811, L33
Wedemeyer-Böhm, S., Scullion, E., Steiner, O., et al. 2012, Natur, 486, 505
Xue, Z., Yan, X., Jin, C., et al. 2019, ApJL, 874, L27
Yang, H., Chae, J., Lim, E.-K., et al. 2013, SoPh, 288, 39
Zaqarashvili, T. V., Khutsishvili, E., Kukhianidze, V., & Ramishvili, G. 2007, A&A, 474, 627
Zhang, Y. Z., Shibata, K., Wang, J. X., et al. 2012, ApJ, 750, 16